ФИЗИКА ЭЛЕМЕНТАРНЫХ ЧАСТИЦ И АТОМНОГО ЯДРА. ТЕОРИЯ

ON THE ISOSPIN EFFECTS IN THE GEOMETRY OF VANISHING FLOW IN HEAVY-ION COLLISIONS

Mandeep Kaur[a], Sakshi Gautam[b, 1]

[a] Department of Physics, Panjab University, Chandigarh-160014, India

[b] Dev Samaj College for Women, Sector 45 B, Chandigarh-160047, India

We study the behavior of the geometry of vanishing flow (GVF) and its system size dependence at different incident energies. We find that the geometry of vanishing flow is sensitive to the incident energy. We also study the role of isospin degree of freedom through Coulomb potential, symmetry energy and nucleon–nucleon cross sections. Our study reveals that isospin degree of freedom through nucleon–nucleon cross section plays a dominant role compared to Coulomb potential and symmetry energy.

Изучается поведение геометрии исчезающего потока и его величины при различных начальных энергиях. Установлена значительная зависимость геометрии исчезающего потока от начальной энергии. Также исследуется роль изоспиновых степеней свободы с помощью учета кулоновского потенциала, энергии симметрии и сечений взаимодействия нуклонов. Показано, что изоспиновые степени свободы, учтенные с помощью сечения взаимодействия нуклонов, играют ведущую роль по сравнению с изоспиновыми эффектами из-за наличия кулоновского потенциала и учета энергии симметрии.

PACS: 25.70.Pq

INTRODUCTION

The collective transverse flow is among the most fundamental observables that has a direct impact on the understanding of medium effects and evolution of a reaction. The collective transverse flow has been reported to be sensitive to the entrance channel parameters such as incident energy of the projectile [1], colliding geometry [2] as well as to the mass of the reacting nuclei [3]. As noted by many authors, energy dependence of the transverse flow led to its disappearance at a particular incident energy labelled as the energy of vanishing flow (EVF) [4]. At EVF, attractive mean field potential balances the repulsive nucleon–nucleon scattering resulting in net disappearance of the flow. The EVF has been found to be sensitive to the mass of the colliding nuclei [5,6]. The colliding geometry, on the other hand, also plays a significant role in the collective flow and its disappearance as well as in various heavy-ion phenomena like multifragmentation, stopping, etc. [7]. As one moves away from the perfectly central collisions, the transverse flow first increases, reaching a maximum at semi-central collisions, then decreases and finally becomes negative at peripheral collisions. This

---

[1] E-mail: sakshigautm@gmail.com

trend can be understood based on the binary collisions. The value of the impact parameter where the collective flow switches from the positive to negative value has been termed as the geometry of vanishing flow (GVF) [8]. At the same time, with the upcoming and existing radioactive ion beam (RIB) facilities around the world [9], isospin physics has been studied extensively during last one decade. The detailed investigations revealed that the isospin effects noted in the collective flow and EVF are due to the competition between the Coulomb potential, symmetry energy and nucleon–nucleon cross section [10]. Though good amount of work has been reported on the isospin effect in transverse momentum and its EVF, no study is available that investigates the isospin effects on GVF.

We, therefore, aim to find out the role of isospin degree of freedom in the GVF. This study is carried out within the framework of isospin-dependent quantum molecular dynamics (IQMD) model [7, 11] which is described briefly below.

1. THE MODEL

The IQMD model treats different charge states of nucleons, deltas and pions explicitly, as inherited from the Vlasov–Uehling–Uhlenbeck (VUU) model. The IQMD model has been used successfully for the analysis of a large number of observables from low to relativistic energies. The isospin degree of freedom enters into the calculations via symmetry potential, cross sections and Coulomb interaction.

In this model, baryons are represented by Gaussian-shaped density distributions

$$f_i(\mathbf{r}, \mathbf{p}, t) = \frac{1}{\pi^2 \hbar^2} \exp\left(-[\mathbf{r} - \mathbf{r}_i(t)]^2 \frac{1}{2L}\right) \exp\left(-[\mathbf{p} - \mathbf{p}_i(t)]^2 \frac{2L}{\hbar^2}\right). \tag{1}$$

The nucleons of the target and projectile interact by two- and three-body Skyrme forces, Yukawa potential and Coulomb interactions. In addition, a symmetry potential between protons and neutrons corresponding to the Bethe–Weizsäcker mass formula has also been included. The hadrons propagate using the Hamilton equations of motion:

$$\frac{d\mathbf{r_i}}{dt} = \frac{d\langle H \rangle}{d\mathbf{p}_i}, \quad \frac{d\mathbf{p}_i}{dt} = -\frac{d\langle H \rangle}{d\mathbf{r}_i}, \tag{2}$$

with

$$\langle H \rangle = \langle T \rangle + \langle V \rangle = \sum_i \frac{p_i^2}{2m_i} + \sum_i \sum_{j>i} \int f_i(\mathbf{r}, \mathbf{p}, t) V^{ij}(\mathbf{r}', \mathbf{r}) f_j(\mathbf{r}', \mathbf{p}', t) \, d\mathbf{r} \, d\mathbf{r}' \, d\mathbf{p} \, d\mathbf{p}'. \tag{3}$$

The baryon potential V^{ij}, in the above relation, reads as

$$V^{ij}(\mathbf{r}' - \mathbf{r}) = V^{ij}_{\text{Skrme}} + V^{ij}_{\text{Yukawa}} + V^{ij}_{\text{Coul}} + V^{ij}_{\text{Sym}} =$$
$$= \left[t_1 \delta(\mathbf{r}' - \mathbf{r}) + t_2 \delta(\mathbf{r}' - \mathbf{r}) \rho^{\gamma-1}\left(\frac{\mathbf{r}' + \mathbf{r}}{2}\right) \right] +$$
$$+ t_3 \frac{\exp\left(|(\mathbf{r}' - \mathbf{r})|/\mu\right)}{(|(\mathbf{r}' - \mathbf{r})|/\mu)} + \frac{Z_i Z_j e^2}{|(\mathbf{r}' - \mathbf{r})|} + t_4 \frac{1}{\varrho_0} T_{3i} T_{3j} \delta(\mathbf{r}_i' - \mathbf{r}_j). \tag{4}$$

Here $t_4 = 4C$ and $C = 32$ MeV, Z_i and Z_j denote the charges of ith and jth baryon, and T_{3i} and T_{3j} are their respective T_3 components (i.e., $1/2$ for protons and $-1/2$ for neutrons).

2. RESULTS AND DISCUSSIONS

For the present study, we simulated several thousand events of the symmetric reactions $^{40}Ca + {}^{40}Ca$, $^{58}Ni + {}^{58}Ni$, $^{93}Nb + {}^{93}Nb$, $^{118}Sn + {}^{118}Sn$ and $^{131}Xe + {}^{131}Xe$ at incident energies between 40 and 150 MeV/nucleon. We used a soft equation of state along with standard energy and isospin-dependent nucleon–nucleon cross section. As noted in [11], the cross section for the neutron–proton scattering is three times larger compared to neutron–neutron or proton–proton cross section (labeled as σ_{iso}). The reactions are followed till the transverse flow saturates.

The «*directed transverse momentum* $\langle p_x^{\mathrm{dir}} \rangle$» used in the calculations reads as [12]

$$\langle p_x^{\mathrm{dir}} \rangle = \frac{1}{A} \sum_{i=1}^{A} \mathrm{sign}\,\{y(i)\}\, p_x(i), \tag{5}$$

where $y(i)$ and $p_x(i)$ are, respectively, the rapidity and momentum of the ith particle.

In Fig. 1, we display the impact parameter dependence of $\langle p_x^{\mathrm{dir}} \rangle$ at 150 (panel *a*), 100 (panel *b*) and 40 (panel *c*) MeV/nucleon for different colliding systems. From the figure, we see that at 100 and 150 MeV/nucleon, $\langle p_x^{\mathrm{dir}} \rangle$ rises as we move away from the central collisions. After reaching a maximum at semi-central geometries, it decreases and finally becomes negative at peripheral collisions due to the absence of binary nucleon–nucleon
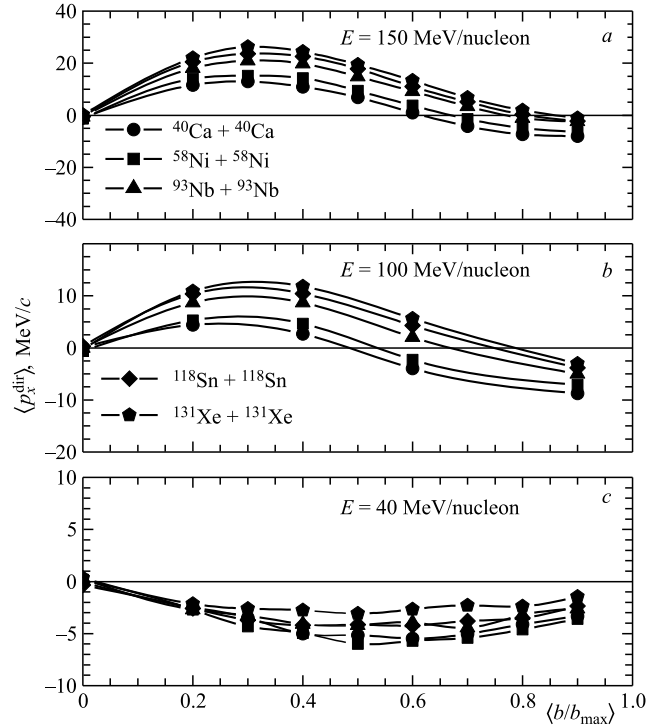

Fig. 1. Impact parameter dependence of transverse in-plane flow $\langle p_x^{\mathrm{dir}} \rangle$ at 150 (*a*), 100 (*b*) and 40 (*c*) MeV/nucleon for various systems. Lines are only to guide eye

collisions. The impact parameter at which the transverse flow becomes zero is labeled as the geometry of vanishing flow (GVF).

On the contrary, at a very low incident energy of 40 MeV/nucleon (Fig. 1, *c*), $\langle p_x^{\mathrm{dir}} \rangle$ remains negative throughout the range of colliding geometry primarily due to the absence of the binary collisions at such a low incident energy. In this case, the attractive mean field keeps transverse momentum in the negative domain for the entire span of the impact parameter. As noted, the transition in the flow from positive to negative values happens at high incident energies of 100 and 150 MeV/nucleon.
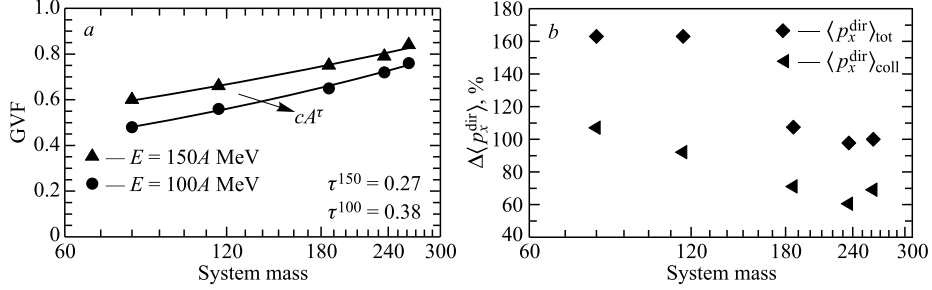

Fig. 2. *a*) System size dependence of the geometry of vanishing flow (GVF) at two incident energies of 100 (circles) and 150 (triangles) MeV/nucleon. Lines represent a power law behavior ($\propto A^\tau$). *b*) The percentage change in $\langle p_x^{\mathrm{dir}} \rangle$ (total (diamonds) and collision contribution (left triangles)) (labeled as $\Delta \langle p_x^{\mathrm{dir}} \rangle$, %) for ^{40}Ca + ^{40}Ca and ^{131}Xe + ^{131}Xe

In Fig. 2, *a*, we display the system size dependence of GVF at incident energies of 100 and 150 MeV/nucleon. From the figure, we see that GVF increases with the increase in the incident energy. As we move towards higher incident energies, enhanced occurrence of binary collisions keeps the transverse flow positive longer and pushes GVF. The rise in the GVF is greater for the lighter systems compared to heavier ones. To see the role of the incident energy in GVF, we further calculated the total $\langle p_x^{\mathrm{dir}} \rangle$ and $\langle p_x^{\mathrm{dir}} \rangle$ due to collisions (labeled as $\langle p_x^{\mathrm{dir}} \rangle_{\mathrm{coll}}$) for the reactions ^{40}Ca + ^{40}Ca and ^{131}Xe + ^{131}Xe. In Fig. 2, *b*, we display the percentage change in total $\langle p_x^{\mathrm{dir}} \rangle$ and in collision contribution at $b/b_{\mathrm{max}} = 0.2$

$$\left(\Delta \langle p_x^{\mathrm{dir}} \rangle \% = \left(\frac{\langle p_x^{\mathrm{dir}} \rangle^{150} - \langle p_x^{\mathrm{dir}} \rangle^{100}}{\langle p_x^{\mathrm{dir}} \rangle^{100}} \right) \cdot 100 \right)$$ in total flow and due to collision contribution.

From the figure, we see that $\Delta \langle p_x^{\mathrm{dir}} \rangle \%$ (for both the total flow and collision contribution) is much larger for lighter nuclei compared to heavier one, although the number of binary collisions scales with the mass of the system. This may be due to the dominance of the Coulomb potential in heavier systems. We also see that GVF follows a mass power law behavior (αA^τ) at both incident energies. The power law parameter τ is 0.27 (labeled as τ^{150}) and 0.38 (labeled as τ^{100}) at 150 and 100 MeV/nucleon, respectively.

Present isospin effects come into picture through three channels, namely, Coulomb potential, symmetry energy and nn cross sections; therefore, as a next step, we investigate the relative importance of all these mechanisms. First, we investigate the role the Coulomb potential plays in GVF and its mass dependence. We calculated the GVF for all colliding systems at 100 MeV/nucleon by excluding the Coulomb potential from our calculations. The results are displayed in Fig. 3 (half-filled circles). From the figure, we see that the omission of Coulomb
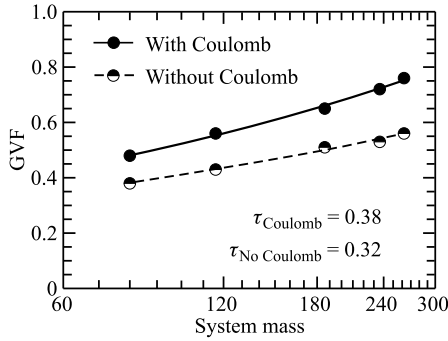
Fig. 3. The system size dependence of GVF without Coulomb potential (half-filled symbols). Here all reactions are performed at an incident energy of 100 MeV/nucleon. Lines represent a power law behavior ($\propto A^\tau$)

potential pushes GVF towards smaller impact parameter. This happens because in the absence of Coulomb potential, repulsive interactions turn out to be weaker. One also notices that the Coulomb potential has a sizeable effect on heavier pair.

Next, we investigate the role of symmetry energy for GVF by calculating the transverse flow for the two extreme pairs of ^{40}Ca + ^{40}Ca (open circles) and ^{131}Xe + ^{131}Xe (open pentagons) without symmetry energy at all colliding geometries. The results are shown in Fig. 4, *a*. From Fig. 4, *a*, we see that the transverse flow decreases at all colliding geometries when the symmetry energy is excluded from the calculations. This is because symmetry energy is repulsive in nature and enhances the in-plane flow. When we switch off symmetry energy, the flow naturally diminishes.
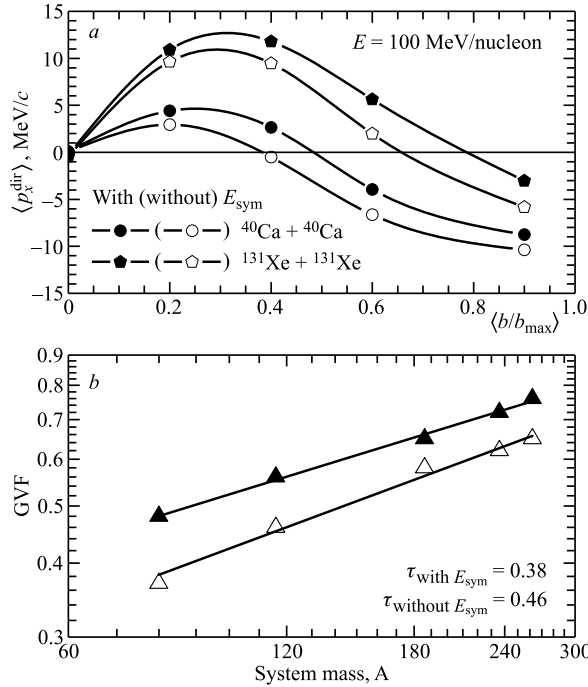
In Fig. 4, *b*, we display the system size dependence of GVF with reference to symmetry energy. From the figure, we see that GVF still follows a mass dependence power law. The power law factor τ now becomes 0.46. From the figure, we see a role of symmetry energy for

Fig. 4. *a*) The impact parameter dependence of $\langle p_x^{\mathrm{dir}} \rangle$ with (closed symbols) and without (open symbols) symmetry energy for the two extreme systems ^{40}Ca + ^{40}Ca (circles) and ^{131}Xe + ^{131}Xe (pentagons). *b*) The system size dependence of GVF without symmetry energy. Lines represent a power law behavior ($\propto A^\tau$)
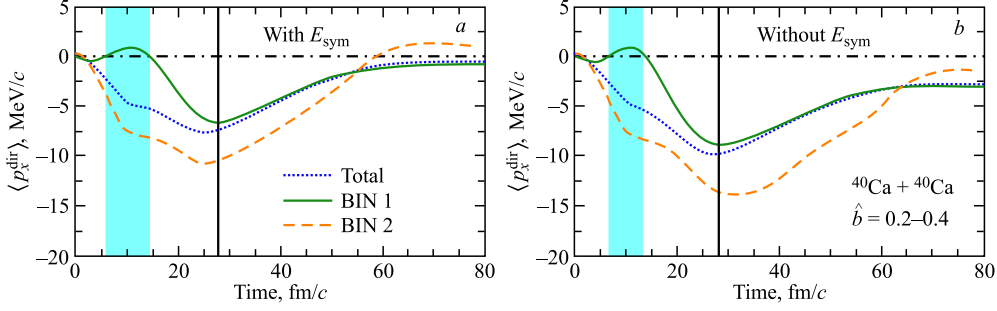
Fig. 5. (Color online) The time evolution of $\langle p_x^{\mathrm{dir}} \rangle$ for $^{40}\mathrm{Ca} + {}^{40}\mathrm{Ca}$ reaction for calculations with (*a*) and without (*b*) symmetry energy at 100 MeV/nucleon. Lines are explained in text

$^{40}\mathrm{Ca} + {}^{40}\mathrm{Ca}$ ($N/Z = 1$), although symmetry energy contribution is not expected to be present in this case. To explore this, we calculated the transverse flow of particles having $\rho/\rho_0 \leqslant 1$ (denoted as BIN 1) and particles having $\rho/\rho_0 > 1$ (denoted as BIN 2), respectively, at all the time steps. The incident energy was taken to be 100 MeV/nucleon. The results are displayed in Fig. 5. Solid (dashed) lines represent the $\langle p_x^{\mathrm{dir}} \rangle$ of particles lying in BIN 1 (BIN 2). Dotted lines represent the total $\langle p_x^{\mathrm{dir}} \rangle$. Panel *a* (*b*) is for calculations with (without) symmetry energy. From the figure, we see that the total $\langle p_x^{\mathrm{dir}} \rangle$ is sensitive to the symmetry energy even for symmetric systems like $^{40}\mathrm{Ca} + {}^{40}\mathrm{Ca}$ with $N/Z = 1$. This is because during the initial stages (between about 5–15 fm/c), the $\langle p_x^{\mathrm{dir}} \rangle$ due to particles in BIN 1 is positive. The duration for which it remains positive is enhanced when we include the symmetry energy (compare shaded area in Figs. 5, *a* and 5, *b*. This is because in the spectator region (where high-rapidity particles are present), the repulsive (attractive) symmetry energy for neutrons (protons) will accelerate the neutrons (protons) away (towards) the overlap zone. Inside the overlap zone, particles are stopped due to binary collisions. Since these particles belong to the same midrapidity region, their momenta (due to symmetry potential) will add up to the zero, thus nullifying the effect of symmetry potential for protons, whereas neutrons will end up in the spectator rapidity region leading to a net transverse momentum due to the effect of symmetry energy. After about 15 fm/c, $\langle p_x^{\mathrm{dir}} \rangle$ of particles lying in the BIN 1 becomes negative because these particles will now be attracted towards the central dense zone. These particles will feel the attractive mean field potential up to about 25 fm/c after which the high-density phase is over. The decrease in the total $\langle p_x^{\mathrm{dir}} \rangle$ due to the attractive mean field potential (between 15–25 fm/c) is less when we include the symmetry potential in our calculations (compare the slopes of dotted curves (total $\langle p_x^{\mathrm{dir}} \rangle$) in Figs. 5, *a* and 5, *b* between the right edge of shaded area and vertical line). This is because the neutrons due to the effect of symmetry energy lie in the spectator rapidity region with momenta away from the overlap zone. The attractive mean field potential will have to decelerate those particles first, make them stop and then accelerate the particles back towards the overlap zone. After about 30 fm/c, the total $\langle p_x^{\mathrm{dir}} \rangle$ follows the $\langle p_x^{\mathrm{dir}} \rangle$ of particles lying in BIN 1 because of the expansion phase of the system. This explains the effect of symmetry energy in a system with $N/Z = 1$.

Further, to see the role of isospin dependence of nucleon–nucleon cross section, we make the cross section isospin-independent by putting $\sigma_{np} = \sigma_{nn}$ or σ_{pp}. The results are displayed in Fig. 6 (labeled as $\sigma_{\mathrm{non\text{-}iso}}$). In Fig. 6, *a*, we display the impact parameter dependence of $\langle p_x^{\mathrm{dir}} \rangle$ for the two extreme systems $^{40}\mathrm{Ca} + {}^{40}\mathrm{Ca}$ (open circles) and $^{131}\mathrm{Xe} + {}^{131}\mathrm{Xe}$ (open

pentagons). From the figure, we see that when we make the cross section isospin-independent, the flow decreases at all impact parameters. This is because the net magnitude of nucleon–nucleon cross section decreases when we make the cross section isospin-independent. From the figure, we also see that the decrease in the flow is more pronounced at semi-central collisions compared to that at peripheral collisions. This is due to the reduction in binary collisions at peripheral geometry, so the effect of isospin dependence of cross section also decreases.
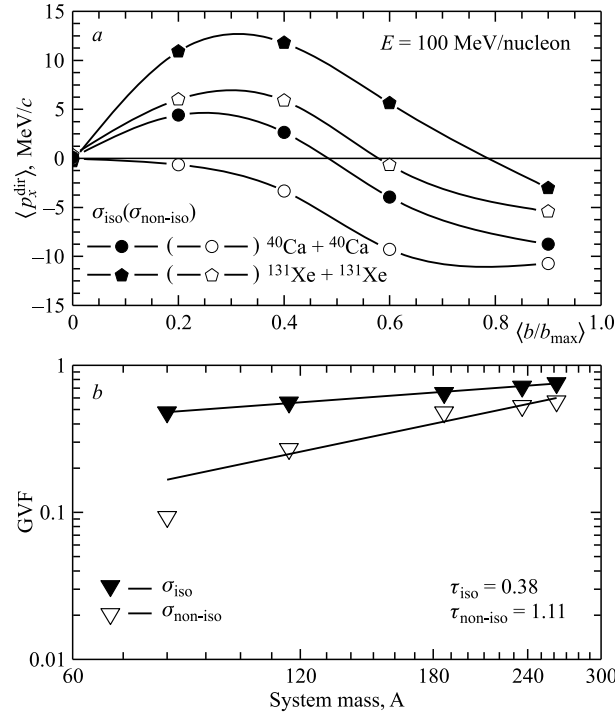

Fig. 6. *a*) The impact parameter dependence of $\langle p_x^{\mathrm{dir}} \rangle$ for isospin-independent nucleon–nucleon cross section for the two extreme systems $^{40}\mathrm{Ca} + ^{40}\mathrm{Ca}$ (open circles) and $^{131}\mathrm{Xe} + ^{131}\mathrm{Xe}$ (open pentagons). *b*) The system size dependence of GVF for isospin-independent nucleon–nucleon cross section (open triangles). Lines represent a power law behavior ($\propto A^{\tau}$)

In Fig. 6, *b*, we display the system size dependence of GVF with isospin-independent nucleon–nucleon cross section (open triangles). From the figure, we see that GVF follows a power law behavior for isospin-independent cross section with power law factor $\tau = 1.11$. GVF decreases by large amount for lighter systems compared to heavier ones, thereby changing the power law parameter by almost a factor of three.

From Figs. 3 and 6, *b*, we noticed that GVF decreases when we exclude the Coulomb potential and also for isospin-independent nn cross section. We also see that the change in the slope of the system size dependence of GVF is greater when we make the cross section isospin-independent. To see the relative strength of the Coulomb potential and nn collisions,

we calculate the flow without Coulomb potential and also without collisions at a fixed incident energy of 100 MeV/nucleon for the reactions ^{40}Ca $+\,^{40}$Ca and ^{131}Xe $+\,^{131}$Xe at $b/b_{\max} = 0.2$ (central collisions) and 0.8 (peripheral). The results are displayed in Fig. 7. From the figure, we see that the flow decreases when we exclude the Coulomb potential (half-filled symbols) and collisions (open symbols) for both central and peripheral collisions. The reduction in the flow due to the Coulomb potential is greater pronounced at peripheral collisions. On the other hand, the flow decreases more at central collisions in the absence of nn collisions because of more relative importance of collisions at central geometries. We also noted that the decrease in the flow is greater when we exclude col-

Fig. 7. The $\langle p_x^{\mathrm{dir}} \rangle$ for ^{40}Ca $+\,^{40}$Ca (circles) and ^{131}Xe $+\,^{131}$Xe (pentagons) without Coulomb potential (half-filled symbols) and without collisions (open) at $b/b_{\max} = 0.2$ and 0.8

lisions at both the colliding geometries than that due to exclusion of Coulomb potential. This indicates that nn collisions have greater role to play compared to the Coulomb potential towards isospin effects.
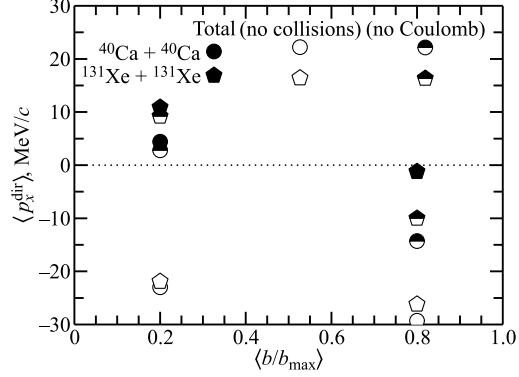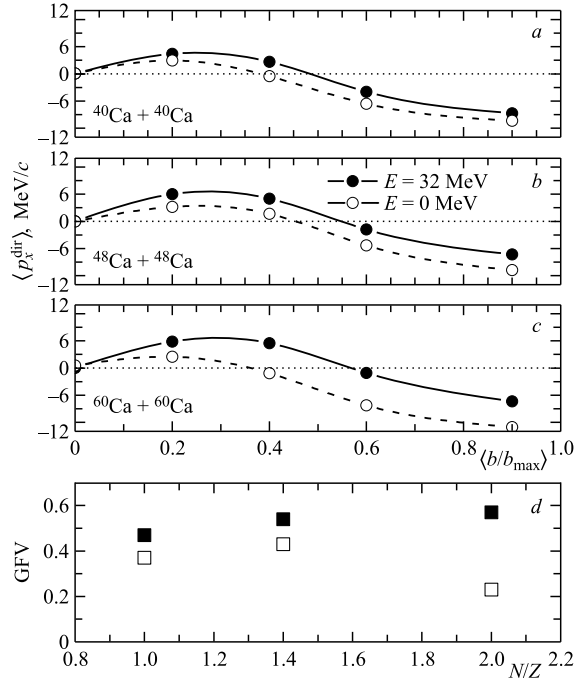

Fig. 8. *a–c*) The impact parameter dependence of $\langle p_x^{\mathrm{dir}} \rangle$ for ^{40}Ca $+\,^{40}$Ca, ^{48}Ca $+\,^{48}$Ca and ^{60}Ca $+\,^{60}$Ca with $E_{\mathrm{sym}} = 32$ (closed symbols) and 0 (open symbols) MeV. *d*) N/Z dependence of GVF

Next, to see the role of symmetry energy in GVF with different neutron contents, we display in Fig. 8 the impact parameter dependence of $\langle p_x^{\mathrm{dir}} \rangle$ for the reactions ^{40}Ca $+ ^{40}$Ca ($N/Z = 1$), ^{48}Ca $+ ^{48}$Ca ($N/Z = 1.4$) and ^{60}Ca $+ ^{60}$Ca ($N/Z = 2$) in panels a, b and c, respectively. From the figure, we see that the flow decreases on reducing the strength of the symmetry energy to zero for all N/Z ratios. In Fig. 8, d, we display the GVF as a function of N/Z of the system. From the figure, we see that the decrease in the GVF increases with the increase in the neutron content of the system due to enhanced role of symmetry energy for higher N/Z ratios.

3. SUMMARY

We have studied the effect of different incident energies on the geometry of vanishing flow and its system size dependence. We have studied the role of isospin degree of freedom by investigating separately the effect of Coulomb potential, symmetry energy and isospin-dependent nucleon–nucleon cross section on the geometry of vanishing flow and its system size dependence. We found significant effect of all the above-mentioned mechanisms. Our calculations predict that the system size dependence of the geometry of vanishing flow is more sensitive to isospin dependence of nucleon–nucleon cross section compared to Coulomb potential and symmetry energy, thus indicating that the geometry of vanishing flow can act as probe to study the role of isospin degree of freedom through nucleon–nucleon cross sections.

REFERENCES

1. *Beavis D. et al.* // Phys. Rev. C. 1992. V. 45. P. 299.

2. *Pan Q., Danielewicz P.* // Phys. Rev. Lett. 1993. V. 70. P. 2062.

3. *Ogilvie C. A. et al.* // Phys. Rev. C. 1989. V. 40. P. 2592;
   Andronic A. et al. // Phys. Rev. C. 2003. V. 67. P. 034907.

4. *Krofcheck D. et al.* // Phys. Rev. Lett. 1989. V. 63. P. 2028.

5. *Majestro D. J., Bauer W., Westfall G. D.* // Phys. Rev. C. 2000. V. 62. P. 041603 and reference therein.

6. *Sood A. D., Puri R. K.* // Eur. Phys. J. A. 2006. V. 30. P. 571;
   Sood A. D., Puri R. K., Aichelin J. // Phys. Lett. B. 2004. V. 594. P. 260;
   Sood A. D., Puri R. K. // Phys. Rev. C. 2006. V. 73. P. 067602; 2009. V. 79. P. 064618;
   Chugh R., Puri R. K. // Phys. Rev. C. 2010. V. 82. P. 014603;
   Kumar S. et al. // Phys. Rev. C. 1998. V. 58. P. 3494;
   Goyal S. et al. // Nucl. Phys. A. 2011. V. 853. P. 164.

7. *Vermani Y. K. et al.* // J. Phys. G: Nucl. Part. Phys. 2009. V. 36. P. 105103; 2010. V. 37. P. 015105;
   Europhys. Lett. 2010. V. 85. P. 62001;
   Vermani Y. K., Goyal S., Puri R. K. // Phys. Rev. C. 2009. V. 79. P. 064613;
   Vermani Y. K. et al. // Nucl. Phys. A. 2010. V. 847. P. 243;
   Puri R. K., Hartnack C., Aichelin J. // Phys. Rev. C. 1996. V. 54. P. 28.

8. *Chugh R., Sood A. D.* // Parmana J. Phys. 2011. V. 77. P. 289;
   Goyal S. // Nucl. Phys. A. 2011. V. 586. P. 154.

9. *Zhan W. et al.* // Intern. J. Mod. Phys. E. 2006. V. 15. P. 1941;
   see, e.g., http:// www.impcas.ac.in/Zhuye/en/htm/247.htm;
   Yano Y. // Nucl. Instr. Meth. B. 2007. V. 261. P. 1009.

10. *Li B. A. et al.* // Phys. Rev. Lett. 1996. V. 76. P. 4492.

11. *Hartnack C. et al.* // Eur. Phys. J. 1998. V. A1. P. 151;
    Hartnack C., Aichelin J. // Phys. Rev. C. 1994. V. 49. P. 2801;
    Kumar S., Puri R. K. // Phys. Rev. C. 2010. V. 81. P. 014611; 014601;
    Kaur V. et al. // Phys. Lett. B. 2011. V. 697. P. 512; Nucl. Phys. A. 2011. V. 861. P. 37;
    Jain A. // Phys. Rev. C. 2011. V. 84. P. 057602;
    Rajni et al. // Ibid. P. 037606.

12. *Khoa D. T. et al.* // Nucl. Phys. A. 1992. V. 548. P. 102;
    Lehmann E. et ak. // Z. Phys. A. 1996. V. 355. P. 55;
    Sood A. D., Puri R. K. // Phys. Rev. C. 2004. V. 70. P. 034611.